JACS
JOURNAL OF THE AMERICAN CHEMICAL SOCIETY
pubs.acs.org/JACS
Article

Systematic Tuning of Rhodamine Spirocyclization for Super-resolution Microscopy

Nicolas Lardon, Lu Wang,* Aline Tschanz, Philipp Hoess, Mai Tran, Elisa D'Este, Jonas Ries, and Kai Johnsson*

Cite This: https://doi.org/10.1021/jacs.1c05004
Read Online

ABSTRACT: Rhodamines are the most important class of fluorophores for applications in live-cell fluorescence microscopy. This is mainly because rhodamines exist in a dynamic equilibrium between a fluorescent zwitterion and a nonfluorescent but cell-permeable spirocyclic form. Different imaging applications require different positions of this dynamic equilibrium, and an adjustment of the equilibrium poses a challenge for the design of suitable probes. We describe here how the conversion of the *ortho*-carboxy moiety of a given rhodamine into substituted acyl benzenesulfonamides and alkylamides permits the systematic tuning of the equilibrium of spirocyclization with unprecedented accuracy and over a large range. This allows one to transform the same rhodamine into either a highly fluorogenic and cell-permeable probe for live-cell-stimulated emission depletion (STED) microscopy or a spontaneously blinking dye for single-molecule localization microscopy (SMLM). We used this approach to generate differently colored probes optimized for different labeling systems and imaging applications.

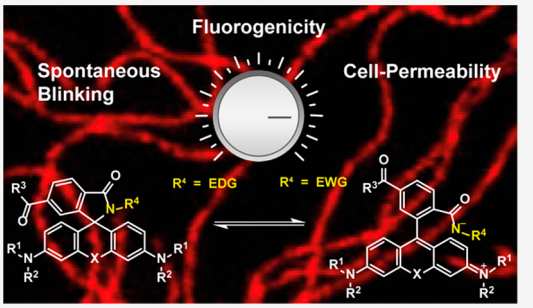

INTRODUCTION

Continuous progress in fluorescence microscopy techniques and labeling strategies has led to an increased demand for suitable fluorescent probes.[1−4] Rhodamine derivatives are a prominent class of fluorophores.[5,6] Their widespread use results from their high photostability and brightness, the broad spectral range they cover, as well as the possibility to tune these properties through synthetic modifications following established procedures.[1,5,7−18] Another crucial feature of rhodamine-based dyes is the capability of spirocyclization.[5,19] They exist in a dynamic equilibrium between a nonfluorescent, cell-permeable spirolactone and a fluorescent zwitterion (Figure 1). Binding of rhodamines to their targets often stabilizes the fluorescent zwitterion relative to the nonfluorescent spirolactone. Consequently, rhodamine-based probes can be fluorogenic, which reduces unspecific background signal.[20] Such cell-permeable and fluorogenic probes are powerful tools for various live-cell microscopy applications.[3] The spirocyclization equilibrium also plays a central role in the design of rhodamine-based probes for single-molecule localization microscopy (SMLM).[21] SMLM techniques rely on the precise detection of individual fluorophores to construct super-resolved images.[2] For this, only a small fraction of the dye population should be in the fluorescent state at the same time, requiring the ability to shift the equilibrium strongly toward the spirocyclic form.[22,23]

To date, strategies to increase cell permeability and fluorogenicity by shifting the equilibrium toward the spirocyclic state were mainly based on modifications of the xanthene core. Exchanging the bridging oxygen of rhodamines with other functionalities (X) altered the state of the equilibrium and created fluorogenic and cell-permeable probes (Figure 1).[27−29] However, this approach leads to rather drastic changes in the equilibrium.[12] Furthermore, it also affects the photophysical properties of the fluorophore, including strong shifts in absorbance and emission wavelengths.[30] Other approaches relied on decreasing the electron density of the xanthene system, for example, through fluorination and introduction of 3-substituted azetidine moieties.[10,11,31] While fluorination of the xanthene core led to a decrease in the quantum yield for certain fluorophores, incorporation of electron-deficient azetidines caused a distinct hypsochromic shift in the absorbance and emission wavelengths.[12,17] Xanthenes with reduced electron density are also known to display enhanced reactivity toward intracellular nucleophiles, which can decrease fluorophore brightness.[16,32,33] Furthermore, modification of the xanthene core can be synthetically challenging and often requires multistep syntheses.[8,12,34,35]

Received: May 14, 2021

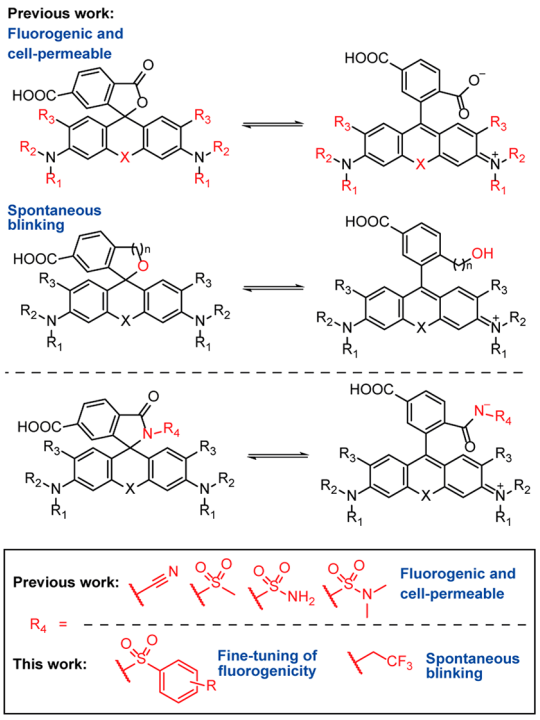

Figure 1. Structures of rhodamine-based fluorophores and their modifications to shift the equilibrium toward the spirocyclic state. Positions colored in red represent structural changes applied to the dye scaffold.

With respect to probes for SMLM techniques, stable rhodamine spirolactams were previously introduced which could be photoactivated to form a fluorescent state.[22,36−38] Another prominent approach is based on replacement of the *ortho*-carboxy moiety with a more nucleophilic hydroxyl group (Figure 1).[31,39−42] The resulting probes can spontaneously switch between their preferred spirocyclic and opened form. Therefore, they exhibit blinking behavior without the need for intense UV irradiation and commonly used additives.[39] Subsequently, spontaneous blinking also was reported for rhodamine spirolactams[43] as well as for photoactivatable spirolactams.[44]

We previously developed a general synthetic strategy to transform rhodamine-based dyes into highly fluorogenic and cell-permeable probes without changing their spectroscopic properties.[20] This was achieved by simple conversion of the *ortho*-carboxy moiety into electron-deficient amides (Figure 1). Here, we show how the equilibrium of spirocyclization can be adjusted much more precisely and over a larger range. Incorporation of benzenesulfonamides with different substituents enabled the systematic fine tuning of the spirocyclization equilibrium and the fluorogenicity of the resulting probes (Figure 1). Furthermore, incorporation of more electron-rich amides allowed the tuning of the equilibrium over a large range and the generation of spontaneously blinking dyes. Thus, the same rhodamine dye can be optimized for applications in either live-cell, no-wash STED imaging or SMLM without changing its spectroscopic properties.

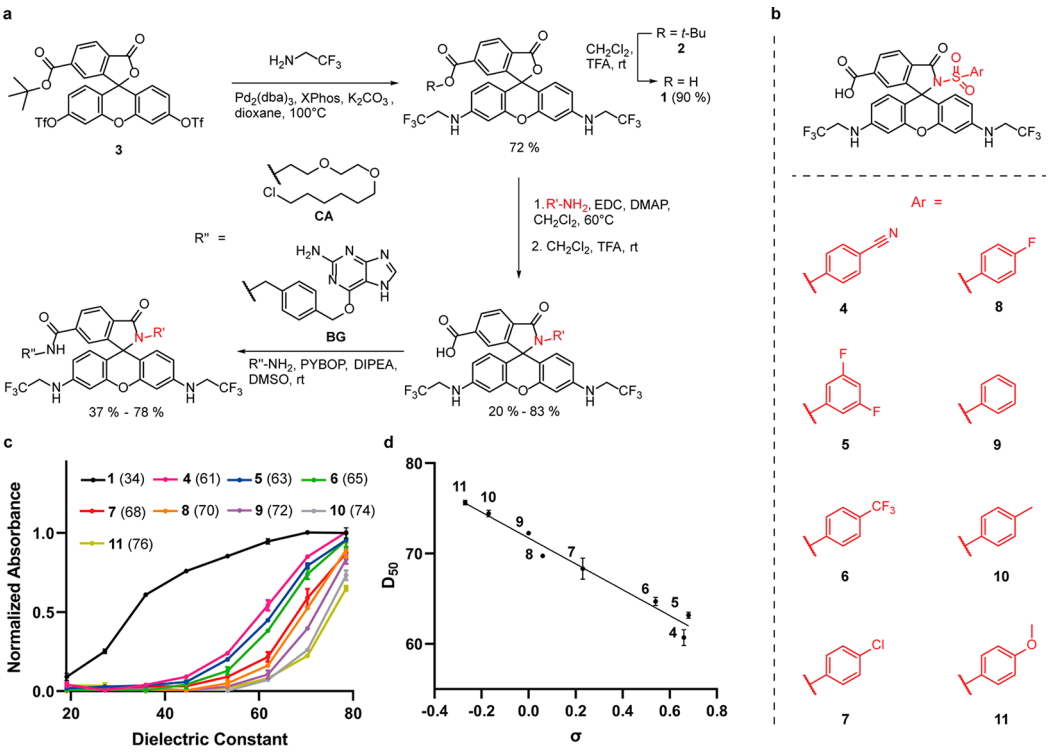

Figure 2. (a) Synthesis of rhodamine 500R derivatives. (b) Structures of rhodamine 500R benzenesulfonamide derivatives (**4**−**11**). (c) Normalized maximal absorbance of **1** and **4**-−**11** (5 μM) in water−dioxane mixtures (v/v 0/100−100/0) at 25 °C as a function of the dielectric constant.[24] Absorbance was normalized to the maximum absorbance of the *ortho*-carboxy dye **1**. Resulting D_{50} values of **1** and **4**−**11** are given in parentheses. (d) Correlation of D_{50} values versus Hammett constants (σ) of the substituents at the benzenesulfonamide.[25] Solid line shows linear regression (R^2 = 0.97). For disubstituted compound **5**, σ of the substituent was doubled.[25,26] Error bars show ± s.d. from 3 experiments.

https://doi.org/10.1021/jacs.1c05004
J. Am. Chem. Soc. XXXX, XXX, XXX−XXX

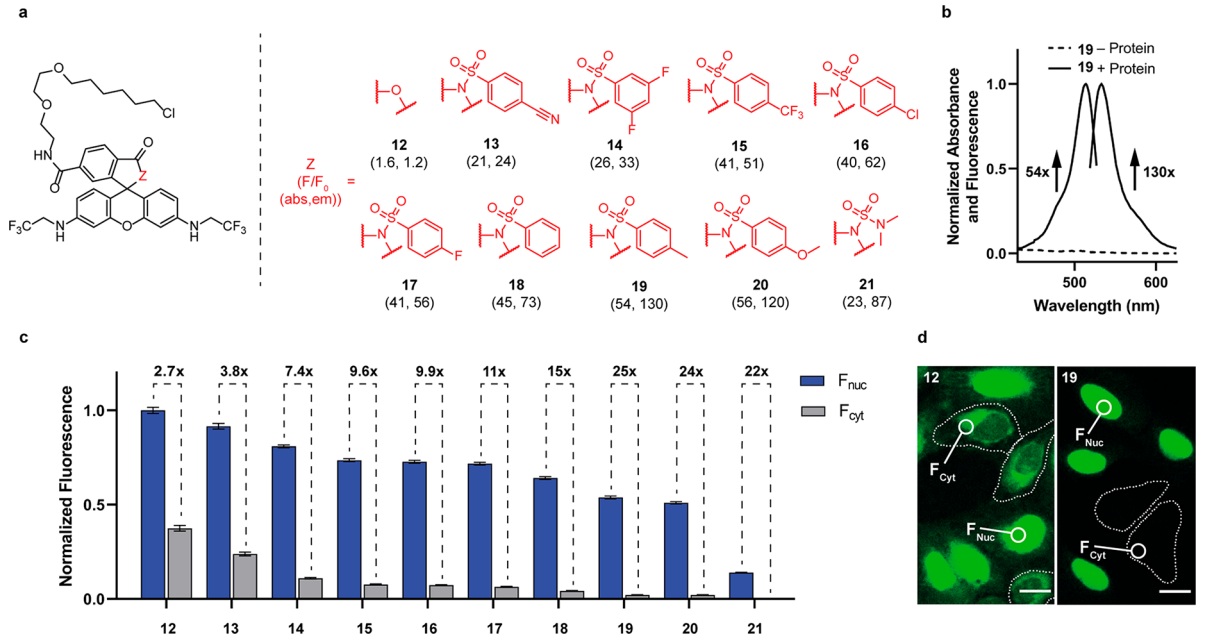

Figure 3. (a) Structures of rhodamine 500R HaloTag probes (**12**–**21**) and absorbance, fluorescence emission turn on upon HaloTag labeling (F/F_0(abs, em)). (b) Normalized absorbance and fluorescence emission spectra of **19** (2.5 μM) in the absence (−Protein) and presence (+Protein) of HaloTag (5 μM) after 2.5 h incubation. (c) Fluorescence ratio (F_{nuc}/F_{cyt}) of **12**–**21** in live-cell, no-wash confocal microscopy. Bar plot representing the normalized nuclear signal (F_{nuc}, U-2 OS FlpIn Halo-SNAP-NLS-expressing cells, normalized to the nuclear signal of SiR-BG) and the cytosolic signal (F_{cyt}, wild-type U-2 OS cells). Cocultured U-2 OS FlpIn Halo-SNAP-NLS-expressing cells and wild-type U-2 OS cells were prelabeled with SiR-BG (500 nM) overnight and then stained with **12**–**21** (200 nM) for 2.5 h. In total, 180 cells were examined from 3 independent experiments for each probe. Error bars show ± s.e.m. (d) Live-cell, no-wash confocal images of cocultured U-2 OS FlpIn Halo-SNAP-NLS-expressing cells and wild-type U-2 OS cells with **12** and **19**. Wild-type U-2 OS cells are represented with dotted lines. Scale bar 20 μm.

RESULTS AND DISCUSSION

Fine Tuning of Rhodamine 500R Spirocyclization. Our goal was to manipulate the spirocyclization equilibrium of a rhodamine-based scaffold such that it can be transformed into different probes that specifically match the requirements of the imaging technique and labeling system. As our synthetic approach modifies the *ortho*-carboxy moiety instead of the xanthene core, we can maintain essential photophysical properties of the original dye. We used rhodamine 500R (**1**), a green fluorophore with a high quantum yield but a low tendency to form the spirolactone, as a platform to test this strategy.[11,17] We synthesized the basic scaffold of rhodamine 500R (**2**) by means of Buchwald−Hartwig amination of **3** (Figure 2a).[8] Amidation of **2** followed by deprotection with TFA yielded a library of different rhodamine 500R spirolactams (Figure 2b and Supplementary Figure 1).[45] Chloroalkane (CA) and O^6-benzylguanine (BG) ligands were coupled to the 6-carboxy group, affording probes for HaloTag and SNAP-tag labeling (Supplementary Figure 1).

The resulting rhodamine 500R benzenesulfonamide derivatives (**4**–**11**) did not reveal distinct changes in the absorbance and emission wavelengths as well as the quantum yield relative to the parental dye, thus confirming that our derivatization strategy does not change the key spectroscopic properties of the underlying rhodamine scaffold (Figure 2b and Supplementary Table 1). Furthermore, we analyzed their spirocyclization behavior by recording the absorbance spectra in dioxane−water mixtures with different dielectric constants (Figure 2c). The D_{50} values derived from these experiments represent the dielectric constant at which one-half of the fluorophore population is in the opened form.[17,20,27] Thus, they are a measure for the state of the spirocyclization equilibrium. We found that incorporation of various benzenesulfonamides led to a distinct shift toward the closed state compared to **1** (Figure 2b and 2c). Furthermore, it enabled fine tuning of the spirocyclization equilibrium with outstanding precision which could not be achieved by the modification of rhodamine 500R with previously reported electron-deficient amines (Figure 2c and Supplementary Figure 2).[20] The linear correlation between the D_{50} values and the Hammett constants (σ) of the aromatic substituents corroborates the rationale of our strategy (Figure 2d). Therefore, benzenesulfonamides bearing electron-donating substituents lead to a stronger shift toward the spirocyclic form than electron-deficient benzenesulfonamides.

Optimizing Rhodamine 500R for HaloTag Labeling. Self-labeling protein tags are useful tools to attach fluorophores to proteins in living cells.[4] HaloTag is a widely used protein tagging system and covalently binds to a synthetic CA ligand which can be conjugated to fluorophores.[46] To obtain high-contrast images without the need for washing steps, a high fluorogenicity of the corresponding HaloTag probe is required.[3]

We investigated whether the fine tuning of the spirocyclization equilibrium also provides control over the fluorogenicity of the corresponding HaloTag probes (**13**–**20**) (Figure 3a). First, the increase in absorbance and fluorescence upon binding to the HaloTag was tested in vitro (F/F_0). Due to the weak fluorogenic character of the original rhodamine 500R HaloTag probe (**12**), labeling of the HaloTag only slightly elevated its absorbance and fluorescence signals (<2-fold). However, we identified various highly fluorogenic probes among **13**–**20**, and the highest turn on was observed for **19**, exhibiting an increase in absorbance of 54-fold and

https://doi.org/10.1021/jacs.1c05004
J. Am. Chem. Soc. XXXX, XXX, XXX−XXX

fluorescence of more than 130-fold (Figure 3a and 3b and Supplementary Figure 3). The fluorogenicity was further evaluated by live-cell, no-wash microscopy of U-2 OS cells which stably express a SNAP-Halo fusion protein localized to the nucleus and wild-type U-2 OS cells.[20] We compared the nuclear signal of these U-2 OS FlpIn Halo-SNAP-NLS-expressing cells (F_{nuc}) with the cytosolic background signal of wild-type U-2 OS cells (F_{cyt}) (Figure 3c and 3d and Supplementary Figure 4). Consistent with the in vitro test, **19** gave the highest nucleus-to-cytosol signal ratio (F_{nuc}/F_{cyt} = 25) whereas **12** showed no significant fluorogenic behavior (F_{nuc}/F_{cyt} = 2.7). Notably, we observed a decrease in nuclear signal intensity with increasing electron density on the benzenesulfonamide. However, since the decrease in background signal intensity was more pronounced, the F_{nuc}/F_{cyt} ratio was highest for **19**. We observed that introduction of too nucleophilic amines significantly decreases the brightness of the fluorophore, as in the case of dimethylsulfamide **21**. These results show that the precise control over the spirocyclization equilibrium permits one to optimize the fluorogenicity of a fluorophore for HaloTag labeling (Supplementary Figure 5).

Optimizing Rhodamine 500R for SNAP-tag Labeling. Another prominent example of a self-labeling protein tag is the SNAP-tag which specifically reacts with BG fluorophore derivatives.[47] Recent studies revealed that SNAP-tag shifts the spirocyclization equilibrium of rhodamines much less to the fluorescent zwitterion than HaloTag, explaining the decreased brightness of certain fluorogenic rhodamines.[48,49] These findings suggest that the optimal position of the spirocyclization equilibrium will differ for probes for SNAP-tag and HaloTag.

We synthesized and tested different rhodamine 500R-derived SNAP-tag probes (**22**–**24**) for their applicability in live-cell, no-wash microscopy (Figure 4a). Measuring the intracellular labeling kinetics of SNAP-tag localized to the nucleus of U-2 OS cells indicated a low cell permeability for the original rhodamine 500R SNAP-tag probe (**22**) (Figure 4b). Furthermore, we observed high background signal intensities for **22** in in vitro turn-on experiments and live-cell, no-wash microscopy (Figure 4c and 4d, Supplementary Figures 6 and 7). The *p*-toluenesulfonamide derivative (**24**), which yielded the highest fluorogenicity as a HaloTag probe (**19**), showed significantly decreased fluorescence signal upon binding to the SNAP-tag (Figure 4b and Supplementary Figure 6). We therefore envisioned using a probe whose equilibrium is slightly shifted toward the zwitterion compared to **24**. Analyzing the performance of **23**, which contains the more electron-deficient 4-fluorobenzenesulfonamide, revealed an increased fluorescence signal upon binding to the SNAP-tag in vitro as well as in cellulo relative to **24** (Figure 4b and Supplementary Figure 6). Furthermore, enhanced cell permeability and a lower cytosolic background signal compared to **22** were detected (Figures 4b–d). Our strategy therefore enables us to adjust the fluorogenicity and cell permeability of rhodamine 500R to transform it into a suitable SNAP-tag probe for live-cell, no-wash microscopy. Both for HaloTag probe **19** and for SNAP-tag probe **23**, stable fluorogenicity in cellulo (F_{nuc}/F_{cyt}) was observed with incubation times ranging from 5 to 24 h (Supplementary Figure 8). This indicates that after saturation in labeling, the incubation time has no significant influence on the fluorogenicity of these probes (Figure 4b and Supplementary Figure 9).

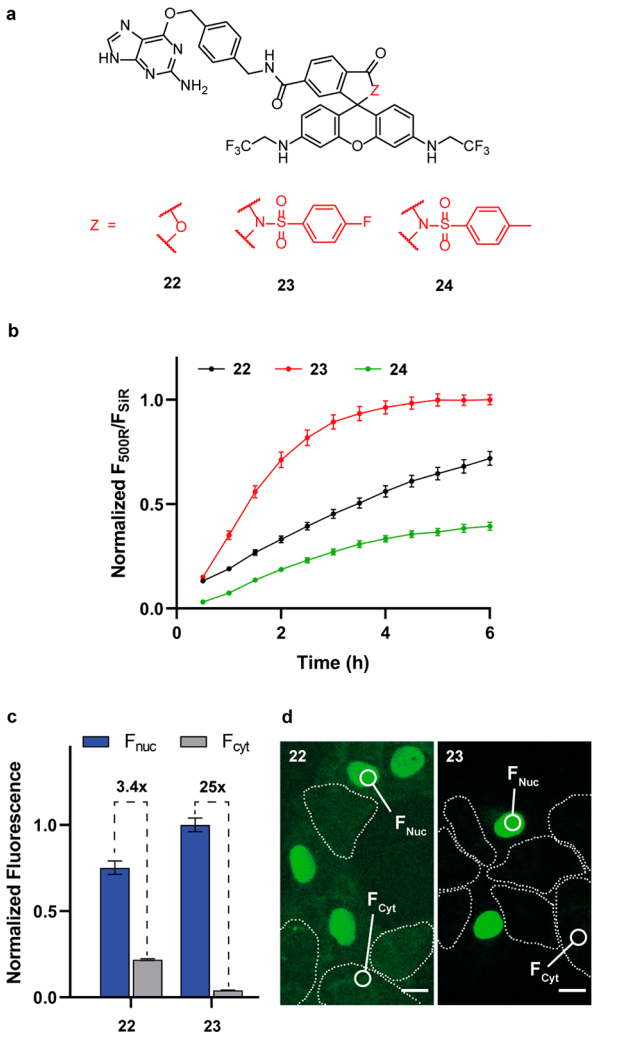

Figure 4. (a) Structures of rhodamine 500R SNAP-tag probes (**22**–**24**). (b) Normalized ratio of rhodamine 500R fluorescence to SiR fluorescence at various time points. U-2 OS FlpIn Halo-SNAP-NLS-expressing cells were prelabeled with SiR-Halo (200 nM) overnight and treated with **22**–**24** (500 nM). In total, 90 cells were examined from 2 independent experiments for each probe. Error bars show ± s.e.m. (c) Fluorescence ratio (F_{nuc}/F_{cyt}) of **22** and **23** in live-cell, no-wash confocal microscopy. Bar plot representing the normalized nuclear signal (F_{nuc}, U-2 OS FlpIn Halo-SNAP-NLS-expressing cells, normalized to the nuclear signal of SiR-Halo) and the cytosolic signal (F_{cyt}, wild-type U-2 OS cells). Cocultured U-2 OS FlpIn Halo-SNAP-NLS-expressing cells and wild-type U-2 OS cells were prelabeled with SiR-Halo (200 nM) overnight and then incubated with **22** and **23** (500 nM) for 5 h. In total, 180 cells were examined from 2 independent experiments for each probe. Error bars show ± s.e.m. (d) Live-cell, no-wash confocal images of cocultured U-2 OS FlpIn Halo-SNAP-NLS-expressing cells and wild-type U-2 OS cells with **22** and **23**. Wild-type U-2 OS cells are represented with dotted lines. Scale bar 20 μm.

Spontaneously Blinking Rhodamine 500R Probe for SMLM. SMLM techniques require probes that switch between a fluorescent and a dark state.[3] In addition to their application as photoswitching probes, recent studies also reported the spontaneous blinking behavior of rhodamine spirolactams.[43,44] Inspired by these findings, we aimed to investigate if our simple synthetic strategy also enables the transformation of rhodamine 500R into a spontaneously blinking probe for SMLM. We envisioned replacing the *ortho*-carboxy group with

https://doi.org/10.1021/jacs.1c05004
J. Am. Chem. Soc. XXXX, XXX, XXX−XXX

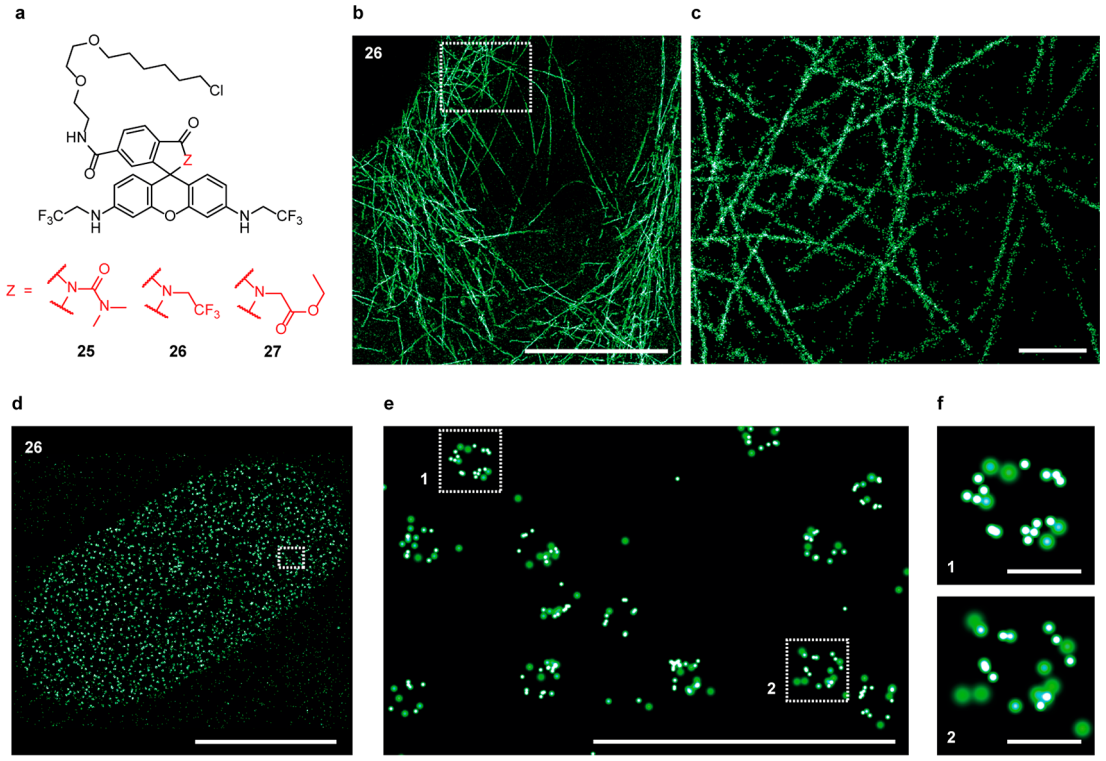

Figure 5. (a) Structures of highly closed rhodamine 500R HaloTag probes (**25**−**27**). (b) Super-resolution image of fixed U-2 OS cells stably expressing Cep41-Halo labeled with **26** (1 μM) overnight. Scale bar 10 μm. (c) Super-resolution image of the marked region in b. Scale bar 1 μm. (d) Super-resolution image of endogenously tagged Nup96-Halo in fixed U-2 OS cells labeled with **26** (1 μM) overnight. Scale bar 10 μm. (e) Super-resolution image of the marked region in d. Scale bar 1 μm. (f) Individual nuclear pores of the marked regions in e. Scale bar 100 nm.

amides with enhanced nucleophilicity, such that only a small fraction of the resulting dye population would be in the fluorescent state at the same time. We therefore synthesized HaloTag probes bearing more nucleophilic amides (**25**− **27**) (Figure 5a). Absorbance measurements at different pH values corroborated that these structural modifications of rhodamine 500R lead to strong shifts in the spirocyclization equilibrium toward the closed state (Supplementary Figure 10). Next, we tested their blinking behavior and performance in SMLM by imaging endogenously tagged Nup96-Halo in fixed U-2 OS cells, a protein present in the nuclear pore complex.[50] After labeling with **25** and **27**, we could not observe discernible nuclear pore structures. However, incubation with **26** enabled visualization of the ring shape of the nuclear pore (Figure 5a and 5d−f). The average photon count of each localization for **26** was 631, and the localization precision peaked at 8.9 nm (Supplementary Figure 11). Furthermore, fixed U-2 OS cells which stably express HaloTag fused to the microtubule (MT) binding protein Cep41 were imaged with **26**.[51] The resulting images showed fine structures of tubulin with a full-width-half-maximum (fwhm) of 40.7 ± 5.7 nm, which is in agreement with previous reports on MT diameter measurements (Figure 5b and 5c and Supplementary Figure 12).[51,52] These observations corroborate the applicability of **26** in SMLM and its spontaneous blinking in standard phosphate-buffered saline (pH 7.4) without the need for short-wavelength irradiation and additives (Supplementary Movies 1 and 2).

Extending the Strategy to Other Rhodamine-Based Dyes. Since our strategy enabled us to transform rhodamine 500R into highly fluorogenic probes specifically optimized for SNAP-tag and HaloTag labeling as well as a blinking dye for SMLM, we investigated whether our approach could be extended to other rhodamine scaffolds. The far-red siliconrhodamine (SiR) scaffold has excellent photophysical properties and therefore represents an interesting target for modification.[27] Due to the high propensity to exist in its spirocyclic state, SiR probes, such as SiR-Halo (**28**), are fluorogenic and cell permeable (Figure 6a).[27] Enhancing the fluorogenicity of **28** even further requires precise fine tuning of the spirocyclization equilibrium. Due to the higher D_{50} value of SiR (D_{50} = 65) compared to that of rhodamine 500R (D_{50} = 34), we envisioned the introduction of an electron-deficient benzenesulfonamide derivative (Figure 2c and Supplementary Figure 13). We therefore synthesized the corresponding probe **29** (Figure 6a).[20] **29** exhibited an increase in fluorescence intensity upon binding to HaloTag of more than 1100-fold in vitro, which is almost a 100-fold higher than the turn on we measured for **28** (Supplementary Figure 14). This simple modification furthermore provided a lower background signal in live-cell imaging without considerably affecting the brightness of the probe bound to HaloTag (Figure 6b and 6c). Specifically, we observed an enhanced nucleus-to-cytosol signal ratio in live-cell, no-wash microscopy of U-2 OS FlpIn Halo-SNAP-NLS-expressing cells and wild-type U-2 OS cells with **29** (F_{nuc}/F_{cyt} = 150) compared to **28** (F_{nuc}/F_{cyt} = 18) (Figure 6b and 6c and Supplementary Figure 15). Next, we used our strategy to modify carborhodamine, an orange fluorophore scaffold with high photostability and brightness.[17] In previous work, we found that replacing the *ortho*-carboxy group of carborhodamine with an acyl dimethylsulfamide delivered a highly fluorogenic HaloTag probe (MaP618-Halo).[20] However, the corresponding SNAP-tag probe (**31**) only showed a negligible increase in fluorescence and absorbance upon binding to the SNAP-tag (Figure 6e and 6f).[20] Thus, our

https://doi.org/10.1021/jacs.1c05004
J. Am. Chem. Soc. XXXX, XXX, XXX−XXX

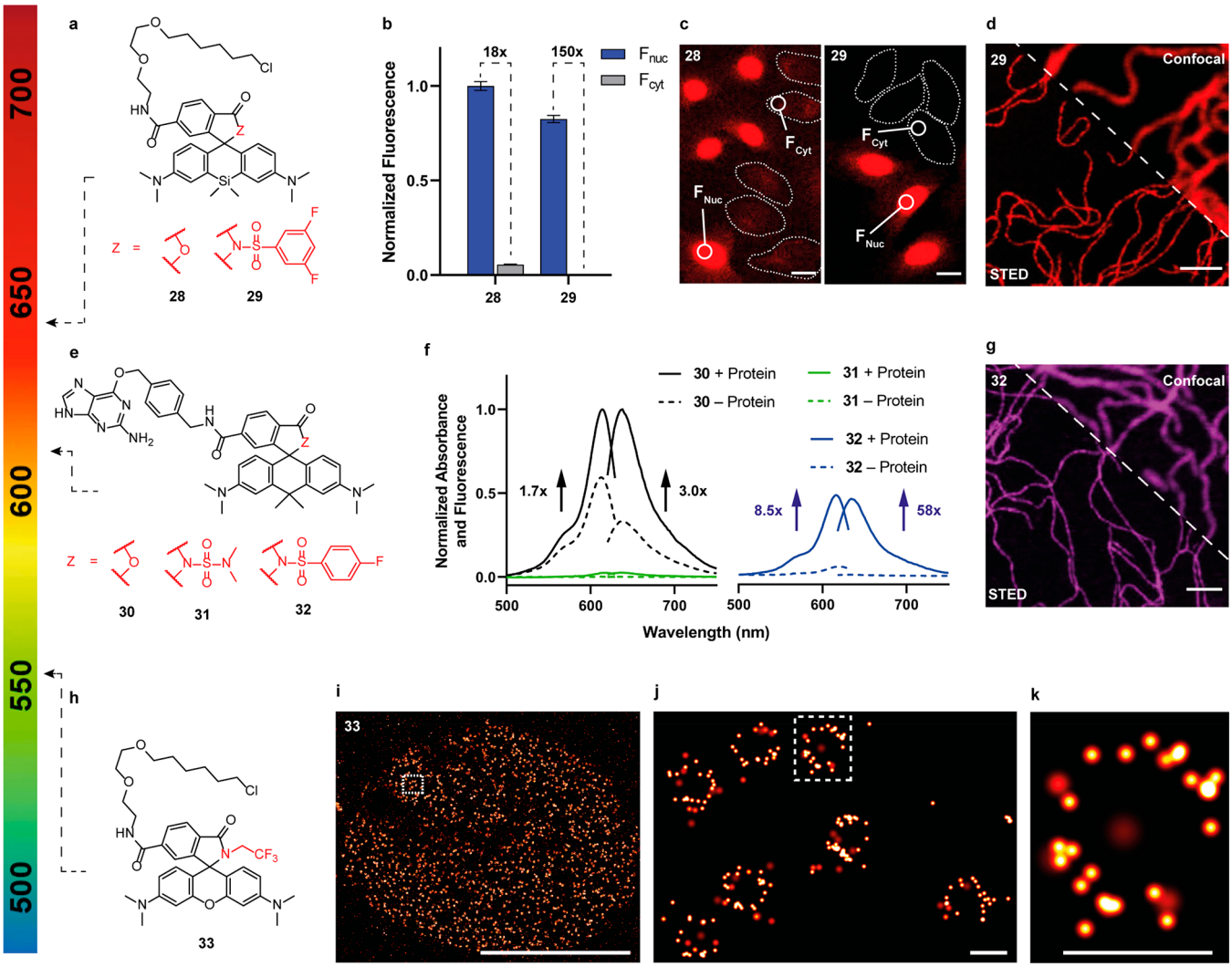

Figure 6. (a) Structures of SiR HaloTag probes (**28** and **29**). (b) Fluorescence ratio (F_{nuc}/F_{cyt}) of **28** and **29** in live-cell, no-wash confocal microscopy. Bar plot representing the normalized nuclear signal (F_{nuc}, U-2 OS FlpIn Halo-SNAP-NLS-expressing cells, normalized to the nuclear signal of **23**) and the cytosolic signal (F_{cyt}, wild-type U-2 OS cells). Cocultured U-2 OS FlpIn Halo-SNAP-NLS-expressing cells and wild-type U-2 OS cells were prelabeled with **23** (500 nM) overnight and then incubated with **28** and **29** (500 nM) for 2.5 h. In total, 180 cells were examined from 2 independent experiments for each probe. Error bars show ± s.e.m. (c) Live-cell, no-wash confocal images of cocultured U-2 OS FlpIn Halo-SNAP-NLS-expressing cells and wild-type U-2 OS cells with **28** and **29**. Wild-type U-2 OS cells are represented with dotted lines. Scale bar 20 μm. (d) Live-cell, no-wash confocal and STED images of U-2 OS Vimentin-Halo-expressing cells labeled with **29** (500 nM) for 2 h. Image data was smoothed with a 1-pixel low-pass Gaussian filter. Scale bar 1.5 μm. (e) Structures of carborhodamine SNAP-tag probes (**30**–**32**). (f) Normalized absorbance and fluorescence emission spectra of **30**–**32** (2.5 μM) in the absence (−Protein) and presence (+Protein) of SNAP-tag (5 μM) after 2.5 h incubation. (g) Live-cell, no-wash confocal and STED images of U-2 OS Vimentin-SNAP-expressing cells labeled with **32** (500 nM) for 4 h. Image data was smoothed with a 1-pixel low-pass Gaussian filter. Scale bar 1.5 μm. (h) Structure of spontaneously blinking TMR HaloTag probe (**33**). (i) Super-resolution image of endogenously tagged Nup96-Halo in fixed U-2 OS cells labeled with **33** (1 μM) overnight. Scale bar 10 μm. (j) Super-resolution image of the marked region in i. Scale bar 100 nm. (k) Individual nuclear pore of the marked region in j. Scale bar 100 nm.

goal was to tune the fluorogenicity of carborhodamine and tailor it into a suitable SNAP-tag probe for live-cell, no-wash microscopy. Carborhodamine (D_{50} = 40) shows a similar D_{50} value compared to rhodamine 500R, indicating a comparable state of the spirocyclization equilibrium (Figure 2c and Supplementary Figure 16). Since incorporation of 4-fluorobenzenesulfonamide transformed rhodamine 500R into a highly fluorogenic SNAP-tag probe (**23**), we also applied this structural change to carborhodamine to obtain **32** (Figure 6e). We then measured the absorbance and fluorescence increase of **32** upon binding to the SNAP-tag in vitro and compared its fluorogenicity to the original carborhodamine SNAP-tag probe (**30**) (Supplementary Figure 17). Despite a reduced brightness, **32** yielded a significantly increased turn-on in the presence of the SNAP-tag compared to **30** (Figure 6f). Live-cell no-wash microscopy of U-2 OS FlpIn Halo-SNAP-NLS-expressing cells and wild-type U-2 OS cells corroborated the enhanced fluorogenicity for **32** (F_{nuc}/F_{cyt} = 65) in comparison to **30** (F_{nuc}/F_{cyt} = 19) (Supplementary Figure 18). While no distinct change between **30** and **32** regarding their intracellular labeling kinetics was detected, we observed that a longer incubation time is required for **29** compared to **28** to reach saturation of the fluorescence signal (Supplementary Figures 19 and 20).

STED microscopy is a powerful method to image cellular structures with high spatial resolution.[53] The parental rhod-

https://doi.org/10.1021/jacs.1c05004
J. Am. Chem. Soc. XXXX, XXX, XXX−XXX

amine 500R, SiR, and carborhodamine dyes of **19**, **29**, and **32** show compatible spectroscopic properties for STED microscopy.[17,54] Since our strategy enhances the fluorogenicity without significantly altering these properties, we tested the applicability of **19**, **29**, and **32** in live-cell, no-wash STED imaging. U-2 OS cells stably expressing Vimentin-Halo were labeled with **19** and **29** as well as Vimentin-SNAP with **32**.[17,55] Images were recorded without prior washing steps and showed bright structures with subdiffraction resolution and exceptionally low background fluorescence (Figure 6d and 6g, Supplementary Figures 21−23).

Finally, we modified tetramethylrhodamine (TMR), a widely used rhodamine scaffold, by means of our strategy to expand the spectrum of colors for spontaneously blinking HaloTag probes (Supplementary Table 5). We converted the *ortho*-carboxy group into a trifluoroethylamide moiety and introduced the CA ligand to obtain HaloTag probe **33** (Figure 6h). We investigated the blinking behavior of **33** and its performance in SMLM by imaging endogenously tagged Nup96-Halo in fixed U-2 OS cells and estimated the duty cycle of **26** and **33** upon labeling immobilized HaloTag on coated glass coverslips (Supplementary Table 6). Analogous to **26**, **33** exhibited spontaneous blinking without the use of short-wavelength irradiation and any additive (Supplementary Movie 3). The resulting super-resolution images revealed the ring shape of the nuclear pores (Figures 6i−k). Furthermore, **33** yielded an average photon count of 2146 per localization, and the localization precision peaked at 3.6 nm (Supplementary Figure 11). A potential explanation for the higher photon count of **33** compared to **26** could be their shifted spirocyclization equilibria (Supplementary Figures 10 and 24). Next, we used **33** to image fixed U-2 OS cells which stably express Cep41-Halo. With this probe, we measured a fwhm of 28.5 ± 5.8 nm, which is compatible with the MT diameter of 25 nm (Supplementary Figure 12). The difference of measured MT diameters between **33** (28.5 ± 5.8 nm) and **26** (40.7 ± 5.7 nm) could be attributed to the difference in localization precision (**26** peaked at 9.9 nm and **33** at 4.8 nm) (Supplementary Figures 11 and 12). However, both results lie within the range of previously reported values.[51,52] Thus, our synthetic approach enabled us to develop **26** and **33**, two spectrally distinct and spontaneously blinking HaloTag probes for SMLM. It is worth noting that similar to what we observed for the fluorogenic SNAP-tag and HaloTag probes, different labeling systems may require different substituents at the spirolactam for the development of spontaneously blinking probes.

CONCLUSIONS

We reported a general strategy that allowed us to adjust the equilibrium of spirocyclization of rhodamines with unprecedented precision and over a large range. We applied this approach to transform rhodamine 500R into highly fluorogenic probes optimized for HaloTag and SNAP-tag labeling as well as a spontaneously blinking probe for SMLM. Furthermore, we extended our strategy to modify various commonly used rhodamines of different colors. The outstanding fluorogenicity and the blinking behavior of the resulting probes, respectively, make them powerful tools for live-cell, no-wash microscopy and SMLM. We envision that the generality of our strategy will allow the transformation of many other rhodamine-based fluorophores into probes that perfectly match the requirements of different imaging techniques and labeling systems.

ASSOCIATED CONTENT

Supporting Information

Supplementary Movies 1−4: Raw camera frames of **26** and **33**. The Supporting Information is available free of charge at https://pubs.acs.org/doi/10.1021/jacs.1c05004.

Supplementary figures and tables; in-vitro tests, cell culture and microscopy; synthesis and characterization; NMR spectra (PDF)

Raw camera frames of **26** in U-2 OS Nup96-Halo cells. Frame rate: 100 fps. (AVI)

Raw camera frames of **26** in U-2 OS Cep41-Halo cells. Frame rate: 100 fs. (AVI)

Raw camera frames of **33** in U-2 OS Nup96-Halo cells. Frame rate: 100 fps. (AVI)

Raw camera frames of **33** in U-2 OS Cep41-Halo cells. Frame rate: 100 fps. (AVI)

AUTHOR INFORMATION

Corresponding Authors

Lu Wang − *Department of Chemical Biology, Max Planck Institute for Medical Research, 69120 Heidelberg, Germany; Key Laboratory of Smart Drug Delivery, Ministry of Education, School of Pharmacy, Fudan University, 201203 Shanghai, China;* orcid.org/0000-0001-8412-2985; Email: Lu.Wang@mr.mpg.de

Kai Johnsson − *Department of Chemical Biology, Max Planck Institute for Medical Research, 69120 Heidelberg, Germany; Institute of Chemical Sciences and Engineering, Ecole Polytechnique Fédérale de Lausanne (EPFL), 1015 Lausanne, Switzerland;* orcid.org/0000-0002-8002-1981; Email: Johnsson@mr.mpg.de

Authors

Nicolas Lardon − *Department of Chemical Biology, Max Planck Institute for Medical Research, 69120 Heidelberg, Germany; Faculty of Chemistry and Earth Sciences, Heidelberg University, 69120 Heidelberg, Germany*

Aline Tschanz − *Cell Biology and Biophysics Unit, European Molecular Biology Laboratory (EMBL), 69117 Heidelberg, Germany; Faculty of Biosciences, Collaboration for Joint PhD Degree between EMBL and Heidelberg University, 69120 Heidelberg, Germany*

Philipp Hoess − *Cell Biology and Biophysics Unit, European Molecular Biology Laboratory (EMBL), 69117 Heidelberg, Germany; Faculty of Biosciences, Collaboration for Joint PhD Degree between EMBL and Heidelberg University, 69120 Heidelberg, Germany*

Mai Tran − *Department of Chemical Biology, Max Planck Institute for Medical Research, 69120 Heidelberg, Germany;* Present Address: M.T.: University of Science-Vietnam National University, 227 Nguyen Van Cu Street, District 5, Ho Chi Minh City 700000, Vietnam

Elisa D'Este − *Optical Microscopy Facility, Max Planck Institute for Medical Research, 69120 Heidelberg, Germany*

Jonas Ries − *Cell Biology and Biophysics Unit, European Molecular Biology Laboratory (EMBL), 69117 Heidelberg, Germany;* orcid.org/0000-0002-6640-9250

Complete contact information is available at: https://pubs.acs.org/10.1021/jacs.1c05004

Notes

The authors declare the following competing financial interest(s): K.J. and L.W. are inventors of the patent Cell-permeable fluorogenic fluorophores which was filed by the Max Planck Society.

■ ACKNOWLEDGMENTS

The authors acknowledge funding of the Max Planck Society. Additional support came from the Deutsche Forschungsgemeinschaft (DFG, German Research Foundation, project number 240245660, SFB 1129, project Z3) to K.J. This research was conducted within the Max Planck School Matter to Life supported by the German Federal Ministry of Education and Research (BMBF) in collaboration with the Max Planck Society (K.J. and N.L.). This work was supported by the European Research Council (CoG-724489 to J.R.) and the European Molecular Biology Laboratory (P.H., A.T., and J.R.). L.W. and M.T. are recipients of an Alexander von Humboldt Fellowship. We thank Andrea Bergner, Bettina Mathes, Jasmine Hubrich, and Ulf Matti for skillful technical assistance, Michelle Frei for helpful discussions, experimental support, and donation of the Cep41-Halo cells, and Stefan Jakobs (Max Planck Institute for Biophysical Chemistry) for donation of the Vimentin-Halo and Vimentin-SNAP cells.

■ REFERENCES

(1) Lavis, L. D. Chemistry Is Dead. Long Live Chemistry! *Biochemistry* **2017**, *56* (39), 5165.
(2) Liu, Z.; Lavis, L. D.; Betzig, E. Imaging Live-Cell Dynamics and Structure at the Single-Molecule Level. *Mol. Cell* **2015**, *58* (4), 644.
(3) Wang, L.; Frei, M. S.; Salim, A.; Johnsson, K. Small-Molecule Fluorescent Probes for Live-Cell Super-Resolution Microscopy. *J. Am. Chem. Soc.* **2019**, *141* (7), 2770.
(4) Xue, L.; Karpenko, I. A.; Hiblot, J.; Johnsson, K. Imaging and manipulating proteins in live cells through covalent labeling. *Nat. Chem. Biol.* **2015**, *11* (12), 917.
(5) Lavis, L. D. Teaching Old Dyes New Tricks: Biological Probes Built from Fluoresceins and Rhodamines. *Annu. Rev. Biochem.* **2017**, *86* (1), 825.
(6) Wang, L.; Du, W.; Hu, Z.; Uvdal, K.; Li, L.; Huang, W. Hybrid Rhodamine Fluorophores in the Visible/NIR Region for Biological Imaging. *Angew. Chem., Int. Ed.* **2019**, *58* (40), 14026.
(7) Panchuk-Voloshina, N.; Haugland, R. P.; Bishop-Stewart, J.; Bhalgat, M. K.; Millard, P. J.; Mao, F.; Leung, W.-Y.; Haugland, R. P. Alexa Dyes, a Series of New Fluorescent Dyes that Yield Exceptionally Bright, Photostable Conjugates. *J. Histochem. Cytochem.* **1999**, *47* (9), 1179.
(8) Butkevich, A. N.; Bossi, M. L.; Lukinavicius, G.; Hell, S. W. Triarylmethane Fluorophores Resistant to Oxidative Photobluing. *J. Am. Chem. Soc.* **2019**, *141* (2), 981.
(9) Grimm, J. B.; English, B. P.; Chen, J.; Slaughter, J. P.; Zhang, Z.; Revyakin, A.; Patel, R.; Macklin, J. J.; Normanno, D.; Singer, R. H.; Lionnet, T.; Lavis, L. D. A general method to improve fluorophores for live-cell and single-molecule microscopy. *Nat. Methods* **2015**, *12* (3), 244.
(10) Grimm, J. B.; Muthusamy, A. K.; Liang, Y.; Brown, T. A.; Lemon, W. C.; Patel, R.; Lu, R.; Macklin, J. J.; Keller, P. J.; Ji, N.; Lavis, L. D. A general method to fine-tune fluorophores for live-cell and in vivo imaging. *Nat. Methods* **2017**, *14* (10), 987.
(11) Mitronova, G. Y.; Belov, V. N.; Bossi, M. L.; Wurm, C. A.; Meyer, L.; Medda, R.; Moneron, G.; Bretschneider, S.; Eggeling, C.; Jakobs, S.; Hell, S. W. New fluorinated rhodamines for optical microscopy and nanoscopy. *Chem. - Eur. J.* **2010**, *16* (15), 4477.
(12) Grimm, J. B.; Tkachuk, A. N.; Xie, L.; Choi, H.; Mohar, B.; Falco, N.; Schaefer, K.; Patel, R.; Zheng, Q.; Liu, Z.; Lippincott-Schwartz, J.; Brown, T. A.; Lavis, L. D. A general method to optimize and functionalize red-shifted rhodamine dyes. *Nat. Methods* **2020**, *17* (8), 815.
(13) Zhou, X.; Lai, R.; Beck, J. R.; Li, H.; Stains, C. I. Nebraska Red: a phosphinate-based near-infrared fluorophore scaffold for chemical biology applications. *Chem. Commun.* **2016**, *52* (83), 12290.
(14) Ren, T.-B.; Xu, W.; Zhang, W.; Zhang, X.-X.; Wang, Z.-Y.; Xiang, Z.; Yuan, L.; Zhang, X.-B. A General Method To Increase Stokes Shift by Introducing Alternating Vibronic Structures. *J. Am. Chem. Soc.* **2018**, *140* (24), 7716.
(15) Koide, Y.; Urano, Y.; Hanaoka, K.; Piao, W.; Kusakabe, M.; Saito, N.; Terai, T.; Okabe, T.; Nagano, T. Development of NIR fluorescent dyes based on Si-rhodamine for in vivo imaging. *J. Am. Chem. Soc.* **2012**, *134* (11), 5029.
(16) Grzybowski, M.; Taki, M.; Senda, K.; Sato, Y.; Ariyoshi, T.; Okada, Y.; Kawakami, R.; Imamura, T.; Yamaguchi, S. A Highly Photostable Near-Infrared Labeling Agent Based on a Phospha-rhodamine for Long-Term and Deep Imaging. *Angew. Chem., Int. Ed.* **2018**, *57* (32), 10137.
(17) Butkevich, A. N.; Mitronova, G. Y.; Sidenstein, S. C.; Klocke, J. L.; Kamin, D.; Meineke, D. N.; D'Este, E.; Kraemer, P. T.; Danzl, J. G.; Belov, V. N.; Hell, S. W. Fluorescent Rhodamines and Fluorogenic Carbopyronines for Super-Resolution STED Microscopy in Living Cells. *Angew. Chem., Int. Ed.* **2016**, *55* (10), 3290.
(18) Song, X.; Johnson, A.; Foley, J. 7-Azabicyclo[2.2.1]heptane as a Unique and Effective Dialkylamino Auxochrome Moiety: Demonstration in a Fluorescent Rhodamine Dye. *J. Am. Chem. Soc.* **2008**, *130* (52), 17652.
(19) Chi, W.; Qi, Q.; Lee, R.; Xu, Z.; Liu, X. A Unified Push−Pull Model for Understanding the Ring-Opening Mechanism of Rhodamine Dyes. *J. Phys. Chem. C* **2020**, *124* (6), 3793.
(20) Wang, L.; Tran, M.; D'Este, E.; Roberti, J.; Koch, B.; Xue, L.; Johnsson, K. A general strategy to develop cell permeable and fluorogenic probes for multicolour nanoscopy. *Nat. Chem.* **2020**, *12* (2), 165.
(21) Li, H.; Vaughan, J. C. Switchable Fluorophores for Single-Molecule Localization Microscopy. *Chem. Rev.* **2018**, *118* (18), 9412.
(22) Belov, V. N.; Bossi, M. L. Photoswitching Emission with Rhodamine Spiroamides for Super-resolution Fluorescence nanoscopies. *Isr. J. Chem.* **2013**, *53* (5), 267.
(23) Sahl, S. J.; Hell, S. W.; Jakobs, S. Fluorescence nanoscopy in cell biology. *Nat. Rev. Mol. Cell Biol.* **2017**, *18* (11), 685.
(24) Critchfield, F. E.; Gibson, J. A.; Hall, J. L. Dielectric Constant for the Dioxane—Water System from 20 to 35°. *J. Am. Chem. Soc.* **1953**, *75* (8), 1991.
(25) Hansch, C.; Leo, A.; Taft, R. W. A survey of Hammett substituent constants and resonance and field parameters. *Chem. Rev.* **1991**, *91* (2), 165.
(26) Bragato, M.; von Rudorff, G. F.; von Lilienfeld, O. A. Data enhanced Hammett-equation: reaction barriers in chemical space. *Chem. Sci.* **2020**, *11* (43), 11859.
(27) Lukinavicius, G.; Umezawa, K.; Olivier, N.; Honigmann, A.; Yang, G.; Plass, T.; Mueller, V.; Reymond, L.; Correa, I. R., Jr.; Luo, Z. G.; Schultz, C.; Lemke, E. A.; Heppenstall, P.; Eggeling, C.; Manley, S.; Johnsson, K. A near-infrared fluorophore for live-cell super-resolution microscopy of cellular proteins. *Nat. Chem.* **2013**, *5* (2), 132.
(28) Lukinavicius, G.; Reymond, L.; D'Este, E.; Masharina, A.; Gottfert, F.; Ta, H.; Guther, A.; Fournier, M.; Rizzo, S.; Waldmann, H.; Blaukopf, C.; Sommer, C.; Gerlich, D. W.; Arndt, H. D.; Hell, S. W.; Johnsson, K. Fluorogenic probes for live-cell imaging of the cytoskeleton. *Nat. Methods* **2014**, *11* (7), 731.
(29) Lukinavicius, G.; Blaukopf, C.; Pershagen, E.; Schena, A.; Reymond, L.; Derivery, E.; Gonzalez-Gaitan, M.; D'Este, E.; Hell, S. W.; Wolfram Gerlich, D.; Johnsson, K. Wolfram Gerlich, D.; Johnsson, K., SiR−Hoechst is a far-red DNA stain for live-cell nanoscopy. *Nat. Commun.* **2015**, *6* (1), 8497.
(30) Koide, Y.; Urano, Y.; Hanaoka, K.; Terai, T.; Nagano, T. Evolution of group 14 rhodamines as platforms for near-infrared

https://doi.org/10.1021/jacs.1c05004
J. Am. Chem. Soc. XXXX, XXX, XXX−XXX

fluorescence probes utilizing photoinduced electron transfer. *ACS Chem. Biol.* **2011**, *6* (6), 600.
(31) Zheng, Q.; Ayala, A. X.; Chung, I.; Weigel, A. V.; Ranjan, A.; Falco, N.; Grimm, J. B.; Tkachuk, A. N.; Wu, C.; Lippincott-Schwartz, J.; Singer, R. H.; Lavis, L. D. Rational Design of Fluorogenic and Spontaneously Blinking Labels for Super-Resolution Imaging. *ACS Cent. Sci.* **2019**, *5* (9), 1602.
(32) Umezawa, K.; Yoshida, M.; Kamiya, M.; Yamasoba, T.; Urano, Y. Rational design of reversible fluorescent probes for live-cell imaging and quantification of fast glutathione dynamics. *Nat. Chem.* **2017**, *9* (3), 279.
(33) Umezawa, K.; Kamiya, M.; Urano, Y. A Reversible Fluorescent Probe for Real-Time Live-Cell Imaging and Quantification of Endogenous Hydropolysulfides. *Angew. Chem., Int. Ed.* **2018**, *57* (30), 9346.
(34) Grimm, J. B.; Brown, T. A.; Tkachuk, A. N.; Lavis, L. D. General Synthetic Method for Si-Fluoresceins and Si-Rhodamines. *ACS Cent. Sci.* **2017**, *3* (9), 975.
(35) Fischer, C.; Sparr, C. Direct Transformation of Esters into Heterocyclic Fluorophores. *Angew. Chem., Int. Ed.* **2018**, *57* (9), 2436.
(36) Fölling, J.; Belov, V.; Kunetsky, R.; Medda, R.; Schönle, A.; Egner, A.; Eggeling, C.; Bossi, M.; Hell, S. W. Photochromic Rhodamines Provide Nanoscopy with Optical Sectioning. *Angew. Chem., Int. Ed.* **2007**, *46* (33), 6266.
(37) Ye, Z.; Yu, H.; Yang, W.; Zheng, Y.; Li, N.; Bian, H.; Wang, Z.; Liu, Q.; Song, Y.; Zhang, M.; Xiao, Y. Strategy to Lengthen the On-Time of Photochromic Rhodamine Spirolactam for Super-resolution Photoactivated Localization Microscopy. *J. Am. Chem. Soc.* **2019**, *141* (16), 6527.
(38) Ho, S. H.; Tirrell, D. A. Enzymatic Labeling of Bacterial Proteins for Super-resolution Imaging in Live Cells. *ACS Cent. Sci.* **2019**, *5* (12), 1911.
(39) Uno, S. N.; Kamiya, M.; Yoshihara, T.; Sugawara, K.; Okabe, K.; Tarhan, M. C.; Fujita, H.; Funatsu, T.; Okada, Y.; Tobita, S.; Urano, Y. A spontaneously blinking fluorophore based on intramolecular spirocyclization for live-cell super-resolution imaging. *Nat. Chem.* **2014**, *6* (8), 681.
(40) Werther, P.; Yserentant, K.; Braun, F.; Kaltwasser, N.; Popp, C.; Baalmann, M.; Herten, D.-P.; Wombacher, R. Live-Cell Localization Microscopy with a Fluorogenic and Self-Blinking Tetrazine Probe. *Angew. Chem., Int. Ed.* **2020**, *59* (2), 804.
(41) Uno, S. N.; Kamiya, M.; Morozumi, A.; Urano, Y. A green-light-emitting, spontaneously blinking fluorophore based on intramolecular spirocyclization for dual-colour super-resolution imaging. *Chem. Commun.* **2018**, *54* (1), 102.
(42) Takakura, H.; Zhang, Y.; Erdmann, R. S.; Thompson, A. D.; Lin, Y.; McNellis, B.; Rivera-Molina, F.; Uno, S.-n.; Kamiya, M.; Urano, Y.; Rothman, J. E.; Bewersdorf, J.; Schepartz, A.; Toomre, D. Long time-lapse nanoscopy with spontaneously blinking membrane probes. *Nat. Biotechnol.* **2017**, *35* (8), 773.
(43) Macdonald, P. J.; Gayda, S.; Haack, R. A.; Ruan, Q.; Himmelsbach, R. J.; Tetin, S. Y. Rhodamine-Derived Fluorescent Dye with Inherent Blinking Behavior for Super-Resolution Imaging. *Anal. Chem.* **2018**, *90* (15), 9165.
(44) Halabi, E. A.; Pinotsi, D.; Rivera-Fuentes, P. Photoregulated fluxional fluorophores for live-cell super-resolution microscopy with no apparent photobleaching. *Nat. Commun.* **2019**, *10* (1), 1232.
(45) Chen, X.; Wu, Q.; Henschke, L.; Weber, G.; Weil, T. An efficient and versatile approach for the preparation of a rhodamine B ester bioprobe library. *Dyes Pigm.* **2012**, *94* (2), 296.
(46) Los, G. V.; Encell, L. P.; McDougall, M. G.; Hartzell, D. D.; Karassina, N.; Zimprich, C.; Wood, M. G.; Learish, R.; Ohana, R. F.; Urh, M.; Simpson, D.; Mendez, J.; Zimmerman, K.; Otto, P.; Vidugiris, G.; Zhu, J.; Darzins, A.; Klaubert, D. H.; Bulleit, R. F.; Wood, K. V. HaloTag: A Novel Protein Labeling Technology for Cell Imaging and Protein Analysis. *ACS Chem. Biol.* **2008**, *3* (6), 373.
(47) Keppler, A.; Gendreizig, S.; Gronemeyer, T.; Pick, H.; Vogel, H.; Johnsson, K. A general method for the covalent labeling of fusion proteins with small molecules in vivo. *Nat. Biotechnol.* **2003**, *21* (1), 86.
(48) Erdmann, R. S.; Baguley, S. W.; Richens, J. H.; Wissner, R. F.; Xi, Z.; Allgeyer, E. S.; Zhong, S.; Thompson, A. D.; Lowe, N.; Butler, R.; Bewersdorf, J.; Rothman, J. E.; St Johnston, D.; Schepartz, A.; Toomre, D. Labeling Strategies Matter for Super-Resolution Microscopy: A Comparison between HaloTags and SNAP-tags. *Cell Chem. Biol.* **2019**, *26* (4), 584.
(49) Wilhelm, J.; Kuehn, S.; Tarnawski, M.; Gotthard, G.; Tuennermann, J.; Taenzer, T.; Karpenko, J.; Mertes, N.; Xue, L.; Uhrig, U.; Reinstein, J.; Hiblot, J.; Johnsson, K. Kinetic and structural characterization of the self-labeling protein tags HaloTag7, SNAP-tag and CLIP-tag. *Biochemistry* **2021**, *60* (33), 2560.
(50) Thevathasan, J. V.; Kahnwald, M.; Cieśliński, K.; Hoess, P.; Peneti, S. K.; Reitberger, M.; Heid, D.; Kasuba, K. C.; Hoerner, S. J.; Li, Y.; Wu, Y.-L.; Mund, M.; Matti, U.; Pereira, P. M.; Henriques, R.; Nijmeijer, B.; Kueblbeck, M.; Sabinina, V. J.; Ellenberg, J.; Ries, J. Nuclear pores as versatile reference standards for quantitative superresolution microscopy. *Nat. Methods* **2019**, *16* (10), 1045.
(51) Frei, M. S.; Hoess, P.; Lampe, M.; Nijmeijer, B.; Kueblbeck, M.; Ellenberg, J.; Wadepohl, H.; Ries, J.; Pitsch, S.; Reymond, L.; Johnsson, K. Photoactivation of silicon rhodamines via a light-induced protonation. *Nat. Commun.* **2019**, *10* (1), 4580.
(52) Ries, J.; Kaplan, C.; Platonova, E.; Eghlidi, H.; Ewers, H. A simple, versatile method for GFP-based super-resolution microscopy via nanobodies. *Nat. Methods* **2012**, *9* (6), 582.
(53) Hell, S. W. Nanoscopy with Focused Light (Nobel Lecture). *Angew. Chem., Int. Ed.* **2015**, *54* (28), 8054.
(54) Bottanelli, F.; Kromann, E. B.; Allgeyer, E. S.; Erdmann, R. S.; Wood Baguley, S.; Sirinakis, G.; Schepartz, A.; Baddeley, D.; Toomre, D. K.; Rothman, J. E.; Bewersdorf, J. Two-colour live-cell nanoscale imaging of intracellular targets. *Nat. Commun.* **2016**, *7* (1), 10778.
(55) Butkevich, A. N.; Ta, H.; Ratz, M.; Stoldt, S.; Jakobs, S.; Belov, V. N.; Hell, S. W. Two-Color 810 nm STED Nanoscopy of Living Cells with Endogenous SNAP-Tagged Fusion Proteins. *ACS Chem. Biol.* **2018**, *13* (2), 475.

https://doi.org/10.1021/jacs.1c05004
J. Am. Chem. Soc. XXXX, XXX, XXX−XXX